Received: 25 September 2019 | Revised: 5 November 2019 | Accepted: 25 November 2019

DOI: 10.1002/mdp2.126

SPECIAL ISSUE ARTICLE

WILEY

Stress corrosion cracking behavior of zirconia ALD–coated AZ31 alloy in simulated body fluid

Mirco Peron | Filippo Berto | Jan Torgersen

Department of Industrial and Mechanical Engineering, Norwegian University of Science and Technology, Trondheim, Norway

Correspondence
Department of Industrial and Mechanical Engineering, Norwegian University of Science and Technology, Richard Birkelands vei 2b, 7034 Trondheim, Norway.
Email: mirco.peron@ntnu.no

Abstract

In the last decades, the interest in magnesium (Mg) and its alloys for biomedical implant devices has been continuously increasing due to their excellent biological and mechanical compatibility with human bones. However, their susceptibility to corrosion-assisted cracking phenomena, such as stress corrosion cracking (SCC) and corrosion fatigue, in presence of the simultaneous action of corrosive human-body-fluid and mechanical loadings has hampered their use in these applications. Developments in this field are thus highly claimed, and this work aims to respond to this need. The effect of a 100-nm-thick zirconia coating produced by means of atomic layer deposition on the SCC susceptibility of AZ31 alloy has in fact been investigated carrying out slow strain rate tests at a strain rate equal to 2.6×10^{-6} s^{-1}. The samples were immersed in simulated body fluid at 37°C for the whole duration of the tests. The presence of the coating has revealed to provide a reduction in the SCC susceptibility, measured by means of the ISCC indexes. The improved SCC behavior of the coated samples has been explained by means of corrosion experiments, ie, potentiodynamic polarization curves and hydrogen evolution experiments.

KEYWORDS

atomic layer deposition, coatings, magnesium alloys, zirconia, stress corrosion cracking

1 | INTRODUCTION

In the past years, due to the increased lifetime in today's world population, the amount of people undergoing surgical procedures involving the implantation of medical devices is continuously growing [1]. In particular, orthopedic surgery is the most important [2–4]. Nowadays, the materials mainly used in orthopedic surgeries are permanent metallic materials, such as stainless steel, titanium, and cobalt-chromium alloys [5]. These materials are characterized by high strength and good corrosion resistance, and they are thus widely used in load-bearing applications [6–8]. However, these permanent materials are characterized by two main drawbacks. First, their elastic modulus is much greater than that of human bone, resulting in the occurrence of the stress-shielding phenomenon [9–15]. Second, permanent metals must be removed from the body when the bone has healed, using a secondary surgical intervention. In fact, even though additional surgeries represent additional costs to the health care system, the prolonged presence of the implant inside the human body can lead to long-term complications, such as local inflammations due to the potential release of cytotoxic ions as a consequence of corrosion or wear processes [16–20]. To overcome these drawbacks, biodegradable materials have been studied, with a particular interest in Mg and its alloys due to their excellent biomechanical compatibility with human bones [21–24]. However, despite their advantages, Mg and its alloys have not yet been used as implant materials because of their high corrosion rates, which may lead to a

loss of mechanical integrity and in hydrogen evolution at a rate that is too fast for the bone tissue to accommodate it. In particular, when high corrosion rates acts concurrently with mechanical loadings, for example, in orthopedic applications, Mg and its alloys are reported to be subjected to corrosion-assisted cracking phenomena, such as stress corrosion cracking (SCC) and corrosion fatigue [25–30]. In particular, SCC is particularly dangerous because it leads to a sudden and catastrophic fast failure under mechanical loading conditions otherwise considered to be safe. Therefore, the development of Mg implants characterized by strength and corrosion resistance high enough to avoid corrosion-assisted cracking phenomena is highly claimed. However, literature in this regard is quite lacking. Peron et al investigated the effect of cryogenic machining on the SCC of AZ31 alloys and reported that the nanosurface layer obtained by the cryogenic machining reduced the SCC susceptibility of more than 10% [31]. More effective in the reduction of the SCC susceptibility has revealed to be the applications of coatings, with a reduction of about 80% in the SCC susceptibility provided by hydroxyapatite coating containing multiwalled carbon nanotubes [32]. Recently, a new coating technique called atomic layer deposition (ALD) has emerged due to its ability to provide dense, high conformal, and pin-hole free films [33,34]. These characteristics result in an efficient improvement in the corrosion resistance of Mg alloys [35]. For example, a 10-nm-thick ZrO_2 coating reduced the corrosion current density of a commercial AZ31 Mg alloy from 5.1×10^{-4} A/cm^2 to 2.7×10^{-7} A/cm^2 [36]. The same decrease of three order of magnitudes has been obtained by Yang et al [37] after coating a Mg-1Sr alloy with 40 nm of ZrO_2. In addition, they reported that the thicker the coating layer, the better the corrosion resistance. However, to the best of the authors' knowledge, the effects of ALD coatings on the SCC susceptibility have not been assessed yet, and thus this work aims to fill this gap. To this aim, AZ31 Mg alloy cylindrical dog-bone samples have been coated with a 100 nm ZrO_2 layer and slow strain rate tests (SSRTs) at strain rate equal to 2.6×10^{-6} s^{-1} have been carried out. The samples were immersed in simulated body fluid (SBF) at 37°C for the whole duration of the tests, and, as reference, the same tests were carried out also in air. The ALD coated samples are found to be less susceptible to SCC than bare samples, and, to understand this different mechanical behavior, the corrosion behavior has been assessed using potentiodynamic polarization curves and hydrogen evolution experiments.

2 | MATERIALS AND METHODS

2.1 | Materials and environments

The material studied in this work is an AZ31 Mg alloy, consisting of a quite homogeneous α matrix and an initial grain size equal to 13.2 ± 8 μm (Figure 1).

The test medium was a SBF prepared according to Ref. 38.

2.2 | Atomic layer deposition

The deposition of a ZrO_2 layer was performed in a commercial ALD reactor (Savannah S200, Veeco Instruments Inc., Massachusetts, USA) through 926 successive cyclic reactions for a total thickness of 100 nm. Each cycle was composed of two parts. The first part consisted of a 250-ms Tetrakis (dimethylamino) zirconium (TDMAZ) precursor pulse and a 10-s Hi-purity N_2 purge with a flow rate of 20 sccm to remove residual reactants and by-products from the chamber so as to prevent any additional chemical vapor deposition reactions. The second part comprised a 150-ms deionized water H_2O precursor pulse and a 15-ms Hi-purity N_2 purge. In the process of deposition, the TDMAZ precursor, H_2O precursor, and delivery lines were heated to 75, 25, and 160°C, respectively.

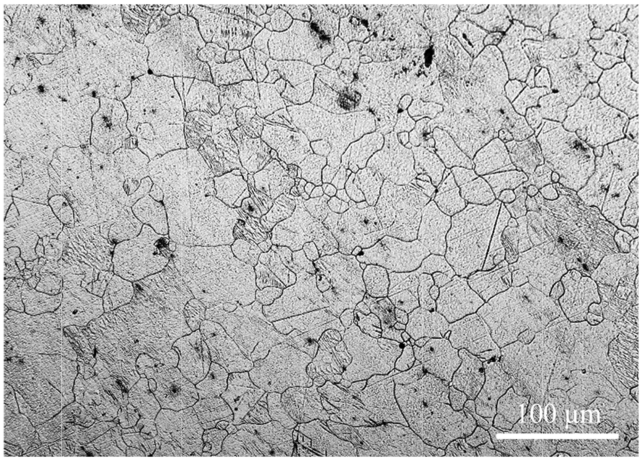

FIGURE 1 Microstructure of the AZ31 alloy in the as-received condition

2.3 | Corrosion tests

2.3.1 | Potentiodynamic polarization curves

The material was received in the form of bars, and these bars were manufactured into disks with a diameter of 29 mm and a thickness of 2 mm using a lathe. The samples were then grounded using a 2000 grit silicon carbide paper and then cleaned with acetone and ethanol. Some of these samples were then coated as described in Section 2.2. The samples so obtained were then electrochemically tested by means of a Gamry Reference 600+ potentiostat using a three-electrode equipment. The bare or the coated samples were immersed in SBF and used as working electrode, while a Hg/Hg_2SO_4 electrode was used as a reference electrode, and a platinum plate electrode as a counter electrode. The area of the samples exposed to SBF was 1 cm^2. The potentiodynamic polarization test was conducted at a stable open-circuit potential after a stabilization period of 30 min. The scan rate of the potentiodynamic polarization test was 0.5 mV/s.

2.3.2 | Immersion tests

According to the procedure described in Ref. 39, the corrosion rate of Mg and its alloys can be assessed by monitoring the hydrogen evolution. In fact, from the corrosion process, one mole of dissolved magnesium release one mole of hydrogen, according to the following equation:

$$Mg + 2H_2O \rightarrow Mg(OH)_2 + H_2 \quad (1)$$

To this aim, cubic samples of side 5 mm were machined from the as-received material and then prepared as described in the previous section. The immersion tests were carried out in SBF at 37°C for 7 days individually.

2.4 | Slow strain rate tests

SSRTs are a common technique used for studying the synergistic effect of stress and corrosion/degradation process on the mechanical properties of a material, and they have been used in this work to investigate the SCC susceptibilities of bare and ZrO_2-coated AZ31 alloy. The tests were carried out using cylindrical dog-bone–shaped samples, whose dimensions are reported in Ref. 31, at a strain rate of 3.5×10^{-6} s^{-1} in SBF solution at body temperature (37 ± 1°C). The tests were carried out according to the standard [40]. The strain rate value was chosen in order to render the Mg alloy susceptible to SCC according to [41], and the experimental set-up is described in details in Ref. 31. In order to quantify the AZ31 SCC sensitivity, the susceptibility indices I_{UTS} and I_ε were calculated according to Equations (2) and (3) [42]:

$$I_{UTS} = \frac{UTS_{air} - UTS_{SBF}}{UTS_{air}} \quad (2)$$

$$I_\varepsilon = \frac{\varepsilon_{air} - \varepsilon_{SBF}}{\varepsilon_{air}} \quad (3)$$

where *UTS* is the ultimate tensile strength and ε the elongation at failure, both evaluated during tests conducted in SBF and air. When the value of the susceptibility index approaches zero, the material is considered to be highly resistant to SCC, namely, the greater the index, the greater the susceptibility to SCC.

3 | RESULTS

3.1 | Potentiodynamic polarization curves

Due to the fact that the corrosion current density (i_{corr}) and the corrosion potentials (E_{corr}) are closely related to the corrosion situation of the sample, the potentiodynamic polarization test has been used to investigate the corrosion properties of materials. The potentiodynamic polarization curves of the coated and bare samples are reported in Figure 2.

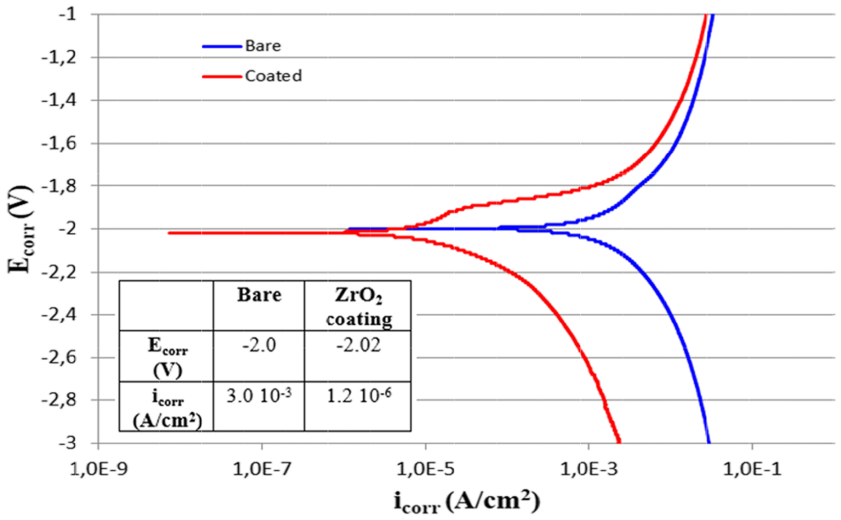

FIGURE 2 Potentiodynamic polarization curves of bare (blue) and coated (red) AZ31 alloy in SBF

Compared with the uncoated alloy, the corrosion current densities of the coated samples display declining trends (Figure 2). Since the lower the corrosion current density, the lower the corrosion rate, a 100-nm ZrO_2 coating is shown to protect Mg alloys from corrosion, which is consistent with previous reports [36,37,43].

3.2 | Immersion tests

As shown in Equation (1), from the dissolution of one mole of magnesium, one mole of hydrogen evolves. In this way, it is possible to assess the corrosion rate of Mg and its alloys by measuring the volume of hydrogen evolved, overcoming the drawbacks of the weight loss method and of the electrochemical techniques can be overcome [39]. From the results of the hydrogen evolution tests (Figure 3), it can be further seen that a 100-nm-thick ZrO_2 coating can prevent the degradation of AZ31 alloy.

3.3 | Slow strain rate tests

The engineering stress-strain curves for the bare and coated AZ31 samples tested in air and in SBF are reported in Figure 4A,B, respectively, with the corresponding UTS and elongation at failure values.

As it can be seen, when tested in air, both the bare and coated samples are characterized by an excellent and comparable combination of strength and ductility. However, when tested in the SBF, the coated samples are characterized by a considerably higher elongation to failure than the bare counterparts.

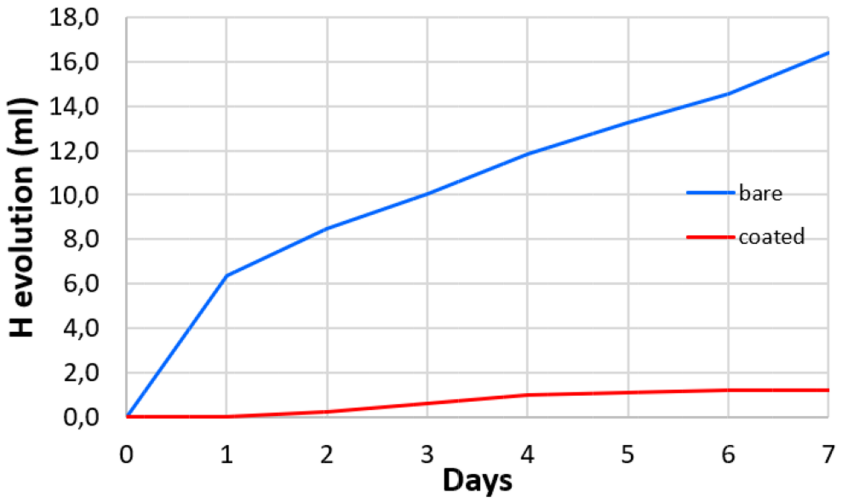

FIGURE 3 Hydrogen evolved from the immersion of bare and coated AZ31 alloy in SBF

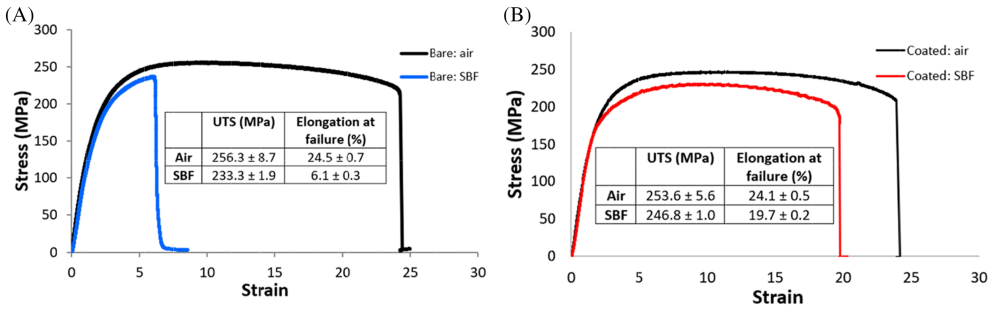

FIGURE 4 Engineering stress-strain curves of bare (A) and coated (B) AZ31 samples tested in air and SBF at 37°C and strain rate of 3.5×10^{-6} s^{-1}

TABLE 1 SCC indices for the bare and coated AZ31 samples

Susceptibility index	Bare	Coated
I_{UTS}	8.97	2.68
I_{ε}	75.1	18.3

To quantify the SCC susceptibility of the bare and coated samples, the I_{UTS} and I_{ε} indices were evaluated and are reported in Table 1.

The SCC indices of the coated samples are lower than those of the bare samples, thus suggesting a higher resistance to SCC in SBF when a 100-nm-thick ZrO_2 coating is applied.

4 | DISCUSSION

The 100-nm thick ZrO_2 coating is shown to highly increase the mechanical performances in presence of a corrosive environment. The I_{UTS} and I_{ε} were in fact reduced of 70.1% and 75.6%, respectively (Table 1). Since SCC in Mg alloys has been attributed to the combination of anodic dissolution and hydrogen embrittlement (HE), it is easily understandable why the coated samples are characterized by a lower SCC susceptibility. Being in fact less hydrogen evolved and being the corrosion less pronounced in the coated samples (Figures 2 and 3), the HE is less pronounced in this samples and thus the material is characterized by a more ductile behavior (Figure 4), providing lower I_{SCC} indices (Table 1). To provide further evidences of this statement, fracture surfaces analyses are now undergoing and will be provided in the future.

5 | CONCLUSION

In this work, to study the effect of a 100-nm-thick ZrO_2 coating on the SCC susceptibility of the AZ31 Mg alloy, SSRTs were carried out in SBF at 37°C on bare and coated samples. In addition, potentiodynamic polarization curves and hydrogen evolution experiments have been carried out to provide an explanation of the observed behavior. The coated samples result to be characterized by a lower SCC susceptibility, in particular, the elongation to failure is more than two times higher than the bare counterparts. This is due to the better corrosion performances provided by the ceramic coating, that, reducing the corrosion rate, allows to reduce the HE phenomenon. To provide further evidences of a lower effect of HE on the coated samples, fracture surfaces analyses are required.

ORCID

Mirco Peron https://orcid.org/0000-0001-6857-8392
Filippo Berto https://orcid.org/0000-0001-9676-9970
Jan Torgersen https://orcid.org/0000-0003-1675-8759

REFERENCES

1. Ginebra MP, Traykova T, Planell JA. Calcium phosphate cements as bone drug delivery systems: A review. J. Control. Release. 2006;113:102-110. https://doi.org/10.1016/j.jconrel.2006.04.007
2. Bradley C., Harrison J.E. Descriptive epidemiology of traumatic fractures in Australia, Australian Institute of Health and Welfare, 2004. https://www.aihw.gov.au/reports/injury/descriptive-epidemiology-traumatic-fractures/contents/table-of-contents ().
3. Long PH. Medical Devices in Orthopedic Applications. Toxicol. Pathol. 2008;36:85-91. https://doi.org/10.1177/0192623307310951
4. Long M, Rack H. Titanium alloys in total joint replacement—a materials science perspective. Biomaterials. 1998;19:1621-1639. https://doi.org/10.1016/S0142-9612(97)00146-4
5. Chen Q, Thouas GA. Metallic implant biomaterials. Mater. Sci. Eng. R Reports. 2015;87:1-57. https://doi.org/10.1016/J.MSER.2014.10.001

6. Hanawa T. Overview of metals and applications. In: *Met. Biomed. Devices*. Elsevier; 2010:3-24 10.1533/9781845699246.1.3.
7. Albrektsson T, Brånemark P-I, Hansson H-A, Lindström J. Osseointegrated Titanium Implants: *Requirements for Ensuring a Long-Lasting, Direct Bone-to-Implant Anchorage in Man*. Acta Orthop. Scand. 1981;52:155-170. https://doi.org/10.3109/17453678108991776
8. Rossi F, Lang NP, De Santis E, Morelli F, Favero G, Botticelli D. Bone-healing pattern at the surface of titanium implants: an experimental study in the dog. Clin. Oral Implants Res. 2014;25:124-131. https://doi.org/10.1111/clr.12097
9. Bauer TW, Schils J. The pathology of total joint arthroplasty. II. Mechanisms of implant failure. Skeletal Radiol. 1999;28:483-497. http://www.ncbi.nlm.nih.gov/pubmed/10525792.
10. Dujovne AR, Bobyn JD, Krygier JJ, Miller JE, Brooks CE. Mechanical compatibility of noncemented hip prostheses with the human femur. J. Arthroplasty. 1993;8:7-22. https://doi.org/10.1016/S0883-5403(06)80102-6
11. Engh CA, Bobyn JD. The influence of stem size and extent of porous coating on femoral bone resorption after primary cementless hip arthroplasty. Clin. Orthop. Relat. Res. 1988;7-28. http://www.ncbi.nlm.nih.gov/pubmed/3370887.
12. Kerner J, Huiskes R, van Lenthe GH, et al. Correlation between pre-operative periprosthetic bone density and post-operative bone loss in THA can be explained by strain-adaptive remodelling. J. Biomech. 1999;32:695-703. https://doi.org/10.1016/S0021-9290(99)00041-X
13. Sumner DR, Galante JO. Determinants of stress shielding: design versus materials versus interface. Clin. Orthop. Relat. Res. 1992;202-212. http://www.ncbi.nlm.nih.gov/pubmed/1729005.
14. Turner TM, Sumner DR, Urban RM, Igloria R, Galante JO. Maintenance of proximal cortical bone with use of a less stiff femoral component in hemiarthroplasty of the hip without cement. An investigation in a canine model at six months and two years. J. Bone Joint Surg. Am. 1997;79:1381-1390. http://www.ncbi.nlm.nih.gov/pubmed/9314401.
15. Van Rietbergen B, Huiskes R, Weinans H, Sumner DR, Turner TM, Galante JO. The mechanism of bone remodeling and resorption around press-fitted THA stems. J. Biomech. 1993;26:369-382. https://doi.org/10.1016/0021-9290(93)90001-U
16. Pound BG. Corrosion behavior of metallic materials in biomedical applications. I. Ti and its alloys. 2014;32:1-20. https://doi.org/10.1515/corrrev-2014-0007
17. Pound BG. Corrosion behavior of metallic materials in biomedical applications. II. Stainless steels and Co-Cr alloys. 2014;32:21-41. https://doi.org/10.1515/corrrev-2014-0008
18. Jacobs JJ, Gilbert JL, Urban RM. Corrosion of metal orthopaedic implants. J. Bone Joint Surg. Am. 1998;80:268-282. http://www.ncbi.nlm.nih.gov/pubmed/9486734.
19. Jacobs JJ, Hallab NJ, Skipor AK, Urban RM. Metal degradation products: a cause for concern in metal-metal bearings? Clin. Orthop. Relat. Res. 2003;139-147. https://doi.org/10.1097/01.blo.0000096810.78689.62
20. Beech IB, Sunner JA, Arciola CR, Cristiani P. Microbially-influenced corrosion: damage to prostheses, delight for bacteria. Int. J. Artif. Organs. 2006;29:443-452. http://www.ncbi.nlm.nih.gov/pubmed/16705614.
21. Peron M, Torgersen J, Berto F. Mg and Its Alloys for Biomedical Applications: Exploring Corrosion and Its Interplay with Mechanical Failure. Metals (Basel). 2017;7:252. https://doi.org/10.3390/met7070252
22. Staiger MP, Pietak AM, Huadmai J, Dias G. Magnesium and its alloys as orthopedic biomaterials: A review. Biomaterials. 2006;27:1728-1734. https://doi.org/10.1016/j.biomaterials.2005.10.003
23. Hänzi A.C, Sologubenko A.S, Uggowitzer P.J. Design strategy for new biodegradable Mg–Y–Zn alloys for medical applications, (2009). http://s3.amazonaws.com/academia.edu.documents/40256888/Design_strategy_for_new_biodegradable_Mg20151122-25584-1a12z48.pdf?AWSAccessKeyId=AKIAIWOWYYGZ2Y53UL3A&Expires=1490954809&Signature=cFqxJQA2%2BJa6em8AhiKnqrACAXo%3D&response-content-disposition=inline%3B filename%3DDesign_strategy_for_new_biodegradable_Mg.pdf ().
24. Singh Raman RK, Jafari S, Harandi SE. Corrosion fatigue fracture of magnesium alloys in bioimplant applications: A review. Eng. Fract. Mech. 2015;137:97-108. https://doi.org/10.1016/j.engfracmech.2014.08.009
25. Teoh S. Fatigue of biomaterials: a review. Int. J. Fatigue. 2000;22:825-837. https://doi.org/10.1016/S0142-1123(00)00052-9
26. Akahori T, Niinomi M, Fukunaga K-I, Inagaki I. Effects of microstructure on the short fatigue crack initiation and propagation characteristics of biomedical α/β titanium alloys. Metall. Mater. Trans. A. 2000;31:1949-1958. https://doi.org/10.1007/s11661-000-0222-z
27. Jafari S, Harandi SE, Singh Raman RK. A review of stress-corrosion cracking and corrosion fatigue of magnesium alloys for biodegradable implant applications. Jom. 2015;67:1143-1153. https://doi.org/10.1007/s11837-015-1366-z
28. Jafari S, Raman RKS, Davies CHJ, Hofstetter J, Uggowitzer PJ, Löffler JF. Stress corrosion cracking and corrosion fatigue characterisation of MgZn1Ca0.3 (ZX10) in a simulated physiological environment. J. Mech. Behav. Biomed. Mater. 2017;65:634-643. https://doi.org/10.1016/J.JMBBM.2016.09.033
29. Kannan MB, Raman RKS. In vitro degradation and mechanical integrity of calcium-containing magnesium alloys in modified-simulated body fluid. Biomaterials. 2008;29:2306-2314. https://doi.org/10.1016/J.BIOMATERIALS.2008.02.003
30. Jafari S, Raman RKS, Davies CHJ. Stress corrosion cracking of an extruded magnesium alloy (ZK21) in a simulated body fluid. Eng. Fract. Mech. 2018;201:47-55. https://doi.org/10.1016/J.ENGFRACMECH.2018.09.002
31. Peron M, Bertolini R, Ghiotti A, Torgersen J, Bruschi S, Berto F. Enhancement of stress corrosion cracking of AZ31 magnesium alloy in simulated body fluid thanks to cryogenic machining. J. Mech. Behav. Biomed. Mater. 2020;101:103429. https://doi.org/10.1016/J.JMBBM.2019.103429
32. Mohajernia S, Pour-Ali S, Hejazi S, Saremi M, Kiani-Rashid A-R. Hydroxyapatite coating containing multi-walled carbon nanotubes on AZ31 magnesium: Mechanical-electrochemical degradation in a physiological environment. Ceram. Int. 2018;44:8297-8305. https://doi.org/10.1016/J.CERAMINT.2018.02.015
33. Graniel O, Weber M, Balme S, Miele P, Bechelany M. Atomic layer deposition for biosensing applications. Biosens. Bioelectron. 2018;122:147-159. https://doi.org/10.1016/J.BIOS.2018.09.038
34. Chalker PR. Photochemical atomic layer deposition and etching. Surf. Coatings Technol. 2016;291:258-263. https://doi.org/10.1016/J.SURFCOAT.2016.02.046
35. Marin E, Lanzutti A, Guzman L, Fedrizzi L. Chemical and electrochemical characterization of TiO2/Al2O3 atomic layer depositions on AZ-31 magnesium alloy. J. Coatings Technol. Res. 2012;9:347-355. https://doi.org/10.1007/s11998-011-9372-8
36. Liu X, Yang Q, Li Z, et al. A combined coating strategy based on atomic layer deposition for enhancement of corrosion resistance of AZ31 magnesium alloy. Appl. Surf. Sci. 2018;434:1101-1111. https://doi.org/10.1016/J.APSUSC.2017.11.032

37. Yang Q, Yuan W, Liu X, et al. Atomic layer deposited ZrO2 nanofilm on Mg-Sr alloy for enhanced corrosion resistance and biocompatibility. Acta Biomater. 2017;58:515-526. https://doi.org/10.1016/J.ACTBIO.2017.06.015
38. Kokubo T, Takadama H. How useful is SBF in predicting in vivo bone bioactivity? Biomaterials. 2006;27:2907-2915. https://doi.org/10.1016/J.BIOMATERIALS.2006.01.017
39. Song G, Atrens A, St John D. An Hydrogen Evolution Method for the Estimation of the Corrosion Rate of Magnesium Alloys. In: *Magnes. Technol. 2001*. Hoboken, NJ, USA: John Wiley & Sons, Inc.; 2013:254-262 10.1002/9781118805497.ch44.
40. ASTM International, ASTM-E466-96. Standard Practice for Slow Strain Rate Testing to Evaluate the Susceptibility of Metallic Materials to Environmentally Assisted Cracking, (n.d.). https://doi.org/10.1520/G0129-00R13.
41. Bobby Kannan M, Dietzel W, Blawert C, Atrens A, Lyon P. Stress corrosion cracking of rare-earth containing magnesium alloys ZE41, QE22 and Elektron 21 (EV31A) compared with AZ80. Mater. Sci. Eng. A. 2008;480:529-539. https://doi.org/10.1016/J.MSEA.2007.07.070
42. Choudhary L, Singh Raman RK, Hofstetter J, Uggowitzer PJ. In-vitro characterization of stress corrosion cracking of aluminium-free magnesium alloys for temporary bio-implant applications. Mater. Sci. Eng. C. 2014;42:629-636. https://doi.org/10.1016/J.MSEC.2014.06.018
43. Liu F, Shan D, Song Y, Han E-H, Ke W. Corrosion behavior of the composite ceramic coating containing zirconium oxides on AM30 magnesium alloy by plasma electrolytic oxidation. Corros. Sci. 2011;53:3845-3852. https://doi.org/10.1016/J.CORSCI.2011.07.037

How to cite this article: Peron M, Berto F, Torgersen J. Stress corrosion cracking behavior of zirconia ALD–coated AZ31 alloy in simulated body fluid. *Mat Design Process Comm*. 2020;2:e126. https://doi.org/10.1002/mdp2.126